



**HAL**  
open science

## Modulation of downstream-propagating waves in aeroacoustic resonance

Daniel Edgington-Mitchell, Daniel J Duke, Tianye Wang, Danielle Harris,  
Oliver Schmidt, Vincent Jaunet, Peter Jordan, Aaron Towne

► **To cite this version:**

Daniel Edgington-Mitchell, Daniel J Duke, Tianye Wang, Danielle Harris, Oliver Schmidt, et al.. Modulation of downstream-propagating waves in aeroacoustic resonance. 25th AIAA/CEAS Aeroacoustics Conference, May 2019, Delft, Netherlands. 10.2514/6.2019-2689 . hal-02378537

**HAL Id: hal-02378537**

**<https://hal.science/hal-02378537>**

Submitted on 25 Nov 2019

**HAL** is a multi-disciplinary open access archive for the deposit and dissemination of scientific research documents, whether they are published or not. The documents may come from teaching and research institutions in France or abroad, or from public or private research centers.

L'archive ouverte pluridisciplinaire **HAL**, est destinée au dépôt et à la diffusion de documents scientifiques de niveau recherche, publiés ou non, émanant des établissements d'enseignement et de recherche français ou étrangers, des laboratoires publics ou privés.

# Modulation of downstream-propagating waves in jet screech.

Daniel Edgington-Mitchell \* Daniel Duke \* Danielle Harris \* Tianye Wang †  
Oliver Schmidt ‡ Vincent Jaunet § Peter Jordan § Aaron Towne †

The coherent component of turbulence in shock-containing flows undergoing aeroacoustic resonance often displays a periodic spatial modulation. This modulation is generally thought to be driven either by the hydrodynamic/acoustic standing wave, or by the shock structures within the jet. In this work, we examine this spatial modulation and seek to determine its cause. Specifically, we consider whether the growth of the Kelvin-Helmholtz wavepackets associated with the resonance cycle is modulated by either of these mechanisms. A combined experimental and theoretical analysis is undertaken. Time-independent velocity snapshots of screeching jets are used to produce a reduced order model for the resonance via a Proper Orthogonal Decomposition. Streamwise Fourier filtering is then applied to isolate the negative and positive wavenumber components, which for this flow correspond to upstream and downstream-propagating waves. A global stability analysis on an experimentally derived base flow is conducted, producing remarkably similar results to those obtained via experiment. In both the global stability analysis and the experimental decomposition, three distinct structures are observed in the spatial wavenumber spectrum. One of these is associated with the downstream-propagating KH mode. One is associated with the upstream component of screech as previously identified. The third component has positive phase velocity, but a radial structure quite different to the other two waves. We provide evidence that this downstream-propagating wave is the result of an interaction between the KH wavepackets and the shocks embedded in the jet, much the same as the upstream-propagating acoustic wave, and has a structure very similar to duct-like modes previously identified in round jets. A weakly-non-parallel local analysis supplements the global analysis, and suggests that the growth of the KH wave is essentially un-modulated by the shocks, at least at the frequencies associated with screech.

## I. Introduction

Shock-containing free shear flows frequently exhibit some form of aeroacoustic resonance, the most well known of these resonant processes are those that produce screech or impingement tones.<sup>1</sup> These resonance processes can be divided into four discrete processes: a downstream-propagating wave,<sup>2-4</sup> a tonal generation mechanism,<sup>5-9</sup> an upstream-propagating wave,<sup>10-15</sup> and a receptivity mechanism.<sup>16-18</sup> Of these, the downstream-propagating wave is the only process where energy is provided to the resonance loop;<sup>2</sup> the growth of the instability wave is driven by the extraction of energy from the mean flow. Amplitude prediction models for aeroacoustic resonance have remained elusive, despite the fact that models for predicting resonant frequencies have been available for many decades.<sup>19</sup> Amongst the many requirements for building such a model, accurate predictions of the downstream-propagating component's growth rate are clearly a high priority.

It is now well established that the initial growth of the Kelvin-Helmholtz wavepacket can be well predicted by the careful application of linear stability theory,<sup>20,21</sup> even for highly turbulent jets (though this usually requires fitting an amplitude parameter).<sup>22</sup> It is less clear how well such linear models perform in shock-containing flows; shocks are by their nature rather non-linear phenomena. It is however recognized that

---

\*Department of Mechanical and Aerospace Engineering, Monash University, Australia

†Department of Mechanical Engineering, University of Michigan, USA

‡Department of Mechanical and Aerospace Engineering, University of California San Diego, USA

§Dept. Fluides, Thermique, Combustion, Institut PPRIME, CNRS - Universite de Poitiers, ENSMA, UPR, Poitiers, France

turbulent structures can undergo significant changes during the passage through a shock wave. Both the shock and the turbulence are influenced by this interaction; the shock becomes locally distorted, while the turbulence sees an amplification of intensity and Reynolds stress.<sup>23</sup> This amplification has been shown to depend on the scale of the turbulence, with finer scales amplified more than large scales. The effect of shocks on turbulence is also anisotropic, with not only the strength but the topology of turbulence altered by the interaction.<sup>24</sup> This interaction may be particularly complicated in the case of the large vortical structures that make up the downstream component of an aeroacoustic resonance process. These structures typically span the sonic line of the jet, meaning some portion of the vortex may pass through the shock cell, whereas components further from the centreline do not. The effect of this interaction (which is also thought to generate much of the shock-associated noise in these jets) on the turbulent wavepacket remains unclear.

An additional source of modulation of the turbulent fluctuations is the standing wave present in the acoustic nearfield of the jet.<sup>25,26</sup> Formed by the interaction of the downstream-propagating hydrodynamic waves and the upstream-propagating acoustic waves, this standing wave is clearly evident in measures of both fluctuating pressure and velocity. In some resonant flows, these upstream-propagating waves can be extremely strong; whether they have any impact on the growth of the downstream-propagating structures is an open question.

In this paper we thus seek to answer the following research question: Is the growth of the downstream-propagating wavepacket in a shock-containing resonant system influenced by either the shocks, or the resonance? To do this we consider three jets undergoing screech, two jets characterized by an  $m = 0$  instability mode, but with shocks of different strength, and one jet whose screech is characterized by an  $m = 1$  helical mode, with much stronger shocks. Several stages of decomposition are applied to an experimentally-derived set of velocity fields. Firstly, all upstream-propagating components are removed from the flow, to suppress the effects of the standing wave. Then, components of the downstream component are considered in isolation and together. A weakly non-parallel linear stability analysis, and a global stability analysis are both performed for the case with the weakest shocks.

## II. Experimental Database

The experimental database used here has been well documented in prior literature. All cases considered are from similar experimental facilities (and the same nozzle), however the details of the velocimetry differ somewhat. Two cases are presented for the  $m = 0$  mode, the A1 and A2 modes of jet screech at pressure ratios of  $NPR = 2.10$  &  $2.25$  respectively.<sup>14</sup> An additional case at a nozzle pressure ratio of  $NPR = 3.40$  is presented, where the flow is characterized by an  $m = 1$  mode associated with the helical C screech mode.<sup>27,28</sup> A summary of the relevant parameters for the jets is presented in Table 1. All jets considered here issue from a purely converging nozzle of diameter  $D = 15mm$ , with a radius of curvature of  $67.15mm$ , ending with a parallel section at the nozzle exit, and an external lip thickness of  $5mm$ . The nozzles are connected to a large plenum chamber; the area ratio between the nozzle and plenum is approximately 100:1. As a consequence of this high contraction ratio, it is expected that the boundary layer at the nozzle exit will be laminar and extremely thin (below the measurement resolution of the PIV system).

**Table 1. Jet Conditions**

$NPR$	$M_j$	$Re$	$St$	Mode
2.10	1.09	$4.4 \times 10^5$	0.65	A1
2.25	1.14	$4.7 \times 10^5$	0.63	A2
3.40	1.45	$8.6 \times 10^5$	0.26	C

For the  $NPR = 2.10$  &  $2.25$  datasets, particle images were obtained using a 12-bit Imperx B4820 camera, with a CCD array of  $4872 \times 3248px$ , at an acquisition frequency of  $2Hz$ . Illumination was provided by a Nd:YAG laser, producing a pair of 6ns pulses of approximately 160mJ, separated by  $\Delta t = 1\mu s$ . For the  $NPR = 3.40$  dataset, particle images were obtained using a pair of PCO 4000 cameras mounted orthogonal to the jet, each with CCD array of  $4008 \times 2760px$ . The resultant velocity fields from the two cameras were stitched together using a convolution with an adaptive Gaussian window<sup>29</sup> using an overlap of 7.5%. Illumination was provided by a Nd:YAG laser, producing a pair of 6ns pulses of approximately 120mJ,

separated by  $\Delta t = 0.8\mu s$ .

Both jets were seeded with  $600nm$  diameter smoke particles,<sup>30</sup> estimated based on observed relaxation times across a normal shock. The pertinent PIV parameters are summarized in Table 2.

**Table 2. Non-dimensional PIV Parameters**

Parameter	Value for NPR = 2.1 or 2.25	Value for NPR = 3.4
$IW_0$	0.12D	0.10D
$IW_1$	0.030D	0.026D
Grid Spacing $\Delta x$	0.01D	0.013D
Depth of Field	0.04D	0.17D
Light Sheet Thickness	0.1D	0.1D
Field of View	5.7D x 3.8D	10D x 2.2 D
Velocity snapshots	10,000	8,000

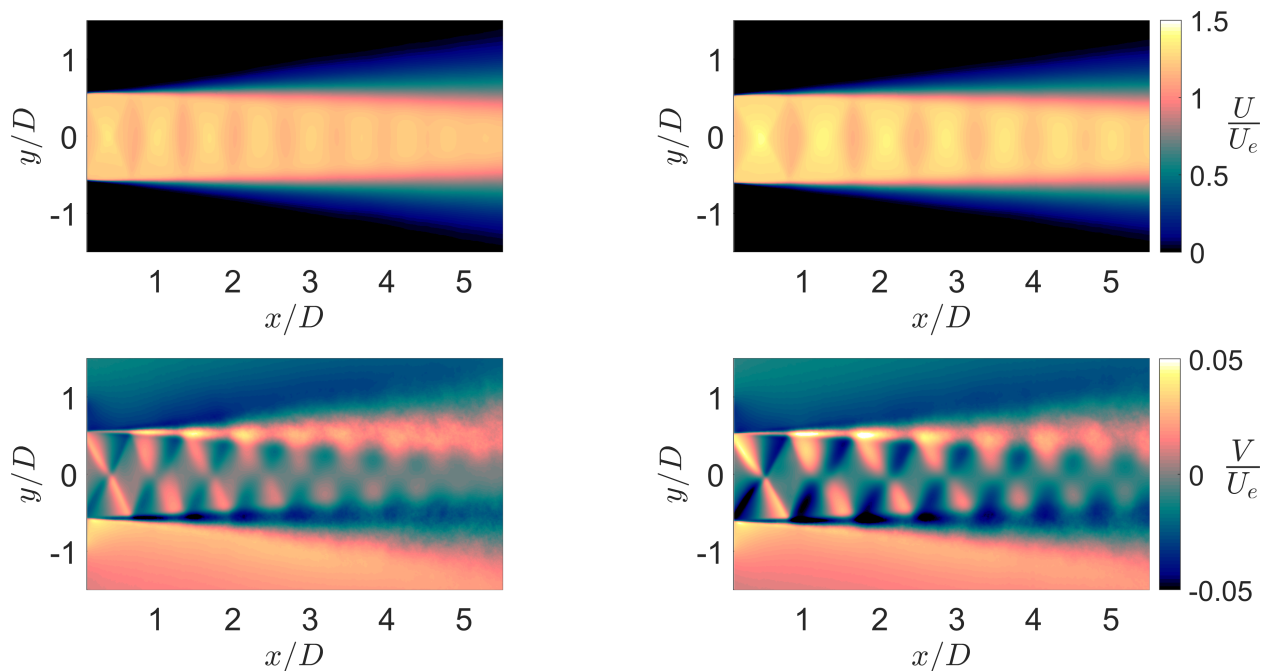


**Figure 1. Mean velocity fields for the two jets characterized by an  $m = 0$  screech tone, operating at  $NPR = 2.10$  and  $NPR = 2.25$ .**

The mean velocity fields for the cases are presented in Figures 1 and 2. For the  $NPR = 2.10$  case, the transverse velocity due to the shocks does not exceed 3% of the jet exit velocity, while for the  $NPR = 3.4$  case the transverse velocity is in excess of 20% of the jet exit velocity.

### III. Methodologies

#### A. Decomposition of Experimental Database

The turbulent wavepackets that comprise the downstream-propagating component of aeroacoustic resonance typically only represent a small percentage of the total turbulent kinetic energy in a flow.<sup>31–33</sup> Eduction of the signatures of these wavepackets from experimental data thus requires some form of modal decomposition.<sup>34</sup>

Proper Orthogonal Decomposition (POD) is the most widely used decomposition method in fluid mechanics broadly,<sup>35,36</sup> and flow resonance in particular.<sup>27,28,37–41</sup> The highly periodic nature of resonant flows makes them particularly amenable to POD, as it is typically possible to reconstruct the entire resonance

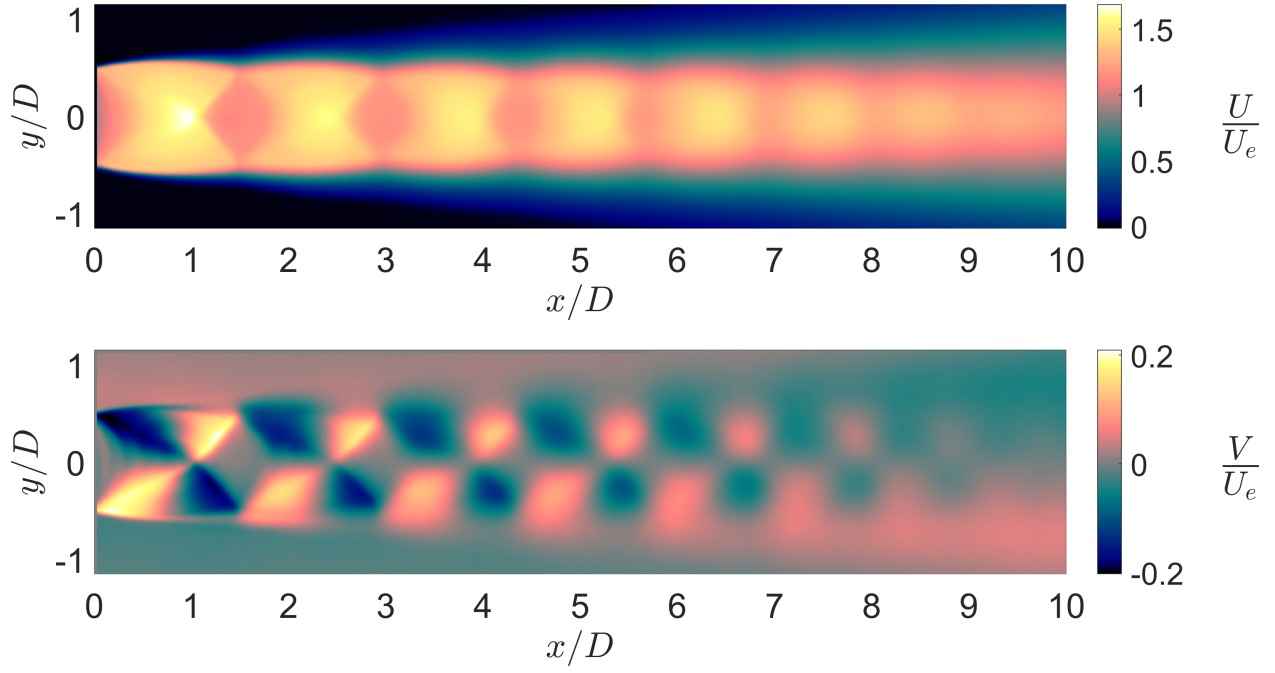


Figure 2. Mean velocity fields for the jet characterized by an  $m = 1$  screech tone, operating at  $NPR = 3.40$ .

cycle from only the leading POD modes;<sup>42</sup> a travelling wave structure will be defined by a pair of POD modes, with a  $90^\circ$  phase offset between them.

The ability of POD to isolate the structures associated with the resonant process enables a triple decomposition on this basis, such that the velocity may be represented as the sum of a mean ( $U$ ), a coherent  $u^c$  and a stochastic  $u''$  component:

$$\mathbf{u}(\mathbf{x}, t) = \mathbf{U}(\mathbf{x}) + \mathbf{u}^c(\mathbf{x}, t) + \mathbf{u}''(\mathbf{x}, t). \quad (1)$$

To educe the coherent component via POD, an autocovariance matrix is constructed from the velocity snapshots  $\mathbf{R} = \mathbf{V}^T \mathbf{V}$ , and the solution of the eigenvalue problem  $\mathbf{R}\mathbf{v} = \lambda\mathbf{v}$  yields the eigenvalues  $\lambda$  and eigenvectors  $\mathbf{v}$  from which the spatial POD modes are constructed as:

$$\phi_n(x, y) = \frac{\mathbf{V}\mathbf{v}_n(t)}{\|\mathbf{V}\mathbf{v}_n(t)\|}, \quad (2)$$

and the coefficients at each time  $t$  for each mode  $n$  can be expressed as

$$\mathbf{a}_n(t) = \mathbf{v}_n(t) \|\mathbf{V}\mathbf{v}_n(t)\|. \quad (3)$$

Since the mode pair represents a periodic phenomenon at the screech frequency  $\omega_s$ , we define:<sup>14,38,42</sup>  $\mathbf{a} = a_1 - ia_2 = \hat{a}e^{-i\omega_s t}$  and  $\boldsymbol{\psi} = \phi_1 + i\phi_2$ . On this basis, with the application of a streamwise Fourier transform, the coherent fluctuations can be represented:

$$\mathbf{q}^c(x, y, t) = \hat{a}e^{-i\omega_s t} \sum_k \hat{\mathbf{q}}_k^c(y) e^{ikx}. \quad (4)$$

Here the temporal Fourier coefficients have been constructed directly from the complex POD mode pair  $\boldsymbol{\psi}$ , such that:

$$\hat{\mathbf{q}}_k^c(y) = \sum_x \boldsymbol{\psi}(x, y) e^{-ikx}. \quad (5)$$

## B. Local stability analysis

The linearized Navier-Stokes equation can be written in the form

$$\frac{\partial \mathbf{q}}{\partial t} + A_x \frac{\partial \mathbf{q}}{\partial x} + A_\theta \frac{\partial \mathbf{q}}{\partial \theta} + A_0 \mathbf{q} = 0. \quad (6)$$

Here, the equations have already been discretized in the radial direction, so the state vector  $\mathbf{q}$  contains all flow variables, e.g., velocities, density, and pressure, at every radial grid point. Applying the normal mode ansatz

$$\mathbf{q}(x, r, \theta, t) = \hat{\mathbf{q}}(r) \exp(ikx + im\theta - i\omega t) \quad (7)$$

leads to the eigenvalue problem

$$(-i\omega I + ikA_x + imA_\theta + A_0) \hat{\mathbf{q}} = 0, \quad (8)$$

where the  $A_{x,\theta,0}$  operators are evaluated at a particular streamwise position  $x_0$ . The azimuthal wavenumber  $m$  is an integer due to the periodicity of the mean jet. For a specified  $m$ , the local eigenmodes of the jet are given by pairs  $(k, \omega)$  and vectors  $\hat{\mathbf{q}}$  satisfying equation (8). Details on the operators and numerics used for the eigenvalue problem are reported elsewhere.<sup>43</sup>

The spatial growth of disturbances can be obtained by choosing real values for the frequency  $\omega$ , and solving the eigenvalue problem for complex-valued wavenumber  $k$ . In particular, the wavepackets discussed previously can be associated with the  $k$  values related to the Kelvin-Helmholtz instability of the mean shear layer. If the the growth rates of the Kelvin-Helmholtz modes match those deduced from the data, it would suggest that the observed modulation is due to a linear interaction between the wavepackets and the shock-cell structure.

## C. Global stability analysis

We also conduct global stability analyses to further explore the reflection process and the resulting resonance and standing waves. The corresponding normal mode ansatz,

$$\mathbf{q}(x, r, \theta, t) = \hat{\mathbf{q}}(x, r) \exp(im\theta - i\omega t), \quad (9)$$

yields a linear system of the form

$$-i\omega \hat{\mathbf{q}} - \mathbf{A}_{x,r} \hat{\mathbf{q}} = \hat{\mathbf{f}}, \quad (10)$$

in which both the streamwise  $x$  and radial  $r$  directions are discretized,  $\mathbf{A}_{x,r}$  is the global linearized Navier-Stokes operator,  $\hat{\mathbf{q}}$  is a state vector consisting of all variables at every grid point in the  $x - r$  domain, and  $\hat{\mathbf{f}}$  is a forcing term that can represent the stochastic component  $u''$  in equation (1) as well as an external input to the system. Equation (10) can be used to explore the linear dynamics of the jet in multiple ways. In this paper, we calculate global modes of the jet, which are given by the eigenvalues of the global linearized Navier-Stokes operator  $\mathbf{A}_{x,r}$ .

# IV. Results

## A. Experimental

The normalized coherent fluctuations ( $|\psi|$ ) for the  $m = 0$  jets are shown in Figure 3, and for the  $m = 1$  jet in Figure 4. The coherent fluctuations are quite similar for the two  $m = 0$  modes, with spatial modulation apparent at both the edges of the shear layer and along the jet centreline. For the  $m = 1$  jet, modulation of the axial velocity component is visible both along the lipline and outside the shear layer, while for the transverse velocity component the strongest modulation is visible along the centreline.

The wavenumber spectra presented in Figure 5 are produced by taking the amplitude of Equation 5. Phase velocity is defined as  $u_p = \omega/k_x$ ; as the POD produces modes correlated to the screech phenomenon, here  $\omega$  is fixed at the screech frequency:  $\omega = \omega_s$ . Thus the sign of  $k_x$  determines the sign of the phase velocity. In our representation, positive values of  $k_x$  are associated with a phase velocity in the downstream direction. The dashed vertical white lines indicate wavenumbers associated with the ambient speed of sound in the upstream and downstream directions, while the dashed vertical red line indicates the wavenumber associated with the average spacing of the shocks in the flow. All three jets have the majority of the energy

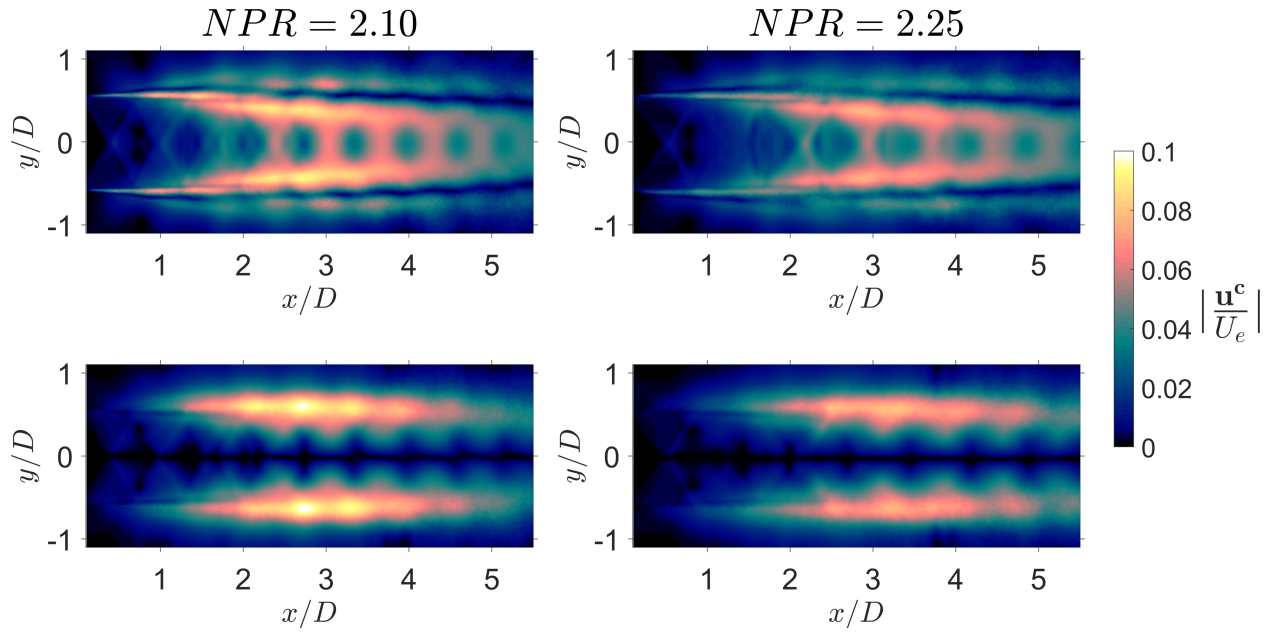


Figure 3. Magnitude of coherent fluctuations for the two jets where the screech mode is an  $m = 0$  azimuthal mode. Upper)  $u = u$ . Lower)  $u = v$ .

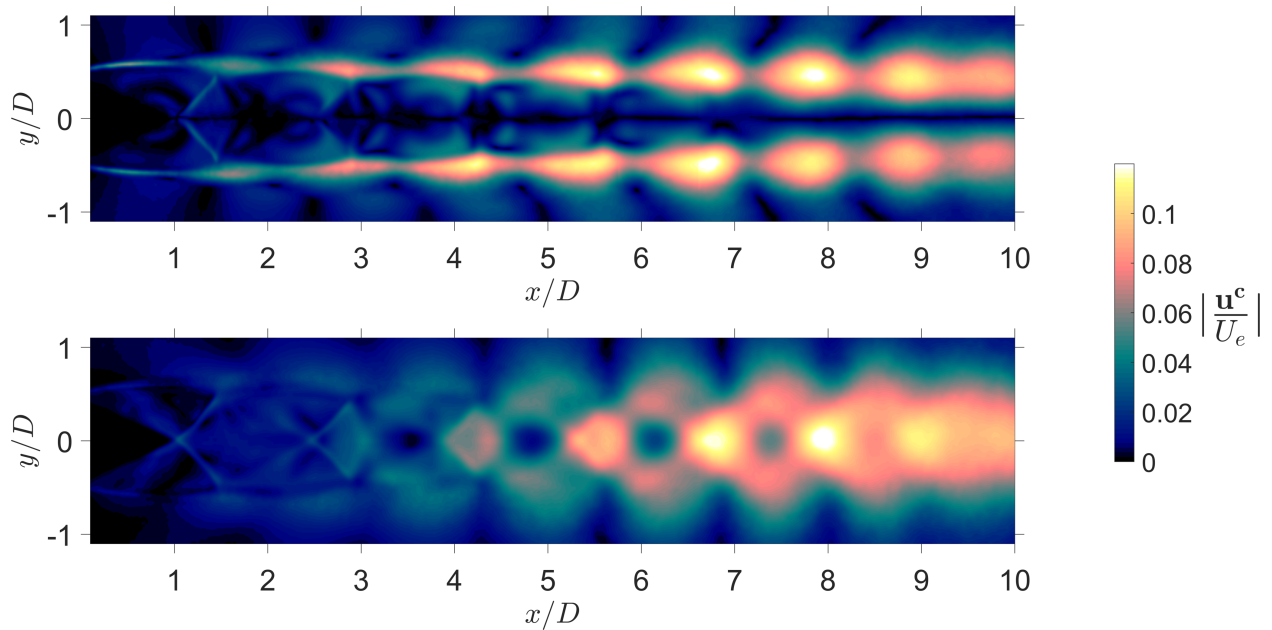


Figure 4. Magnitude of coherent fluctuations for jet where the screech mode is an  $m = 1$  azimuthal mode. Upper)  $u = u$ . Lower)  $u = v$ .

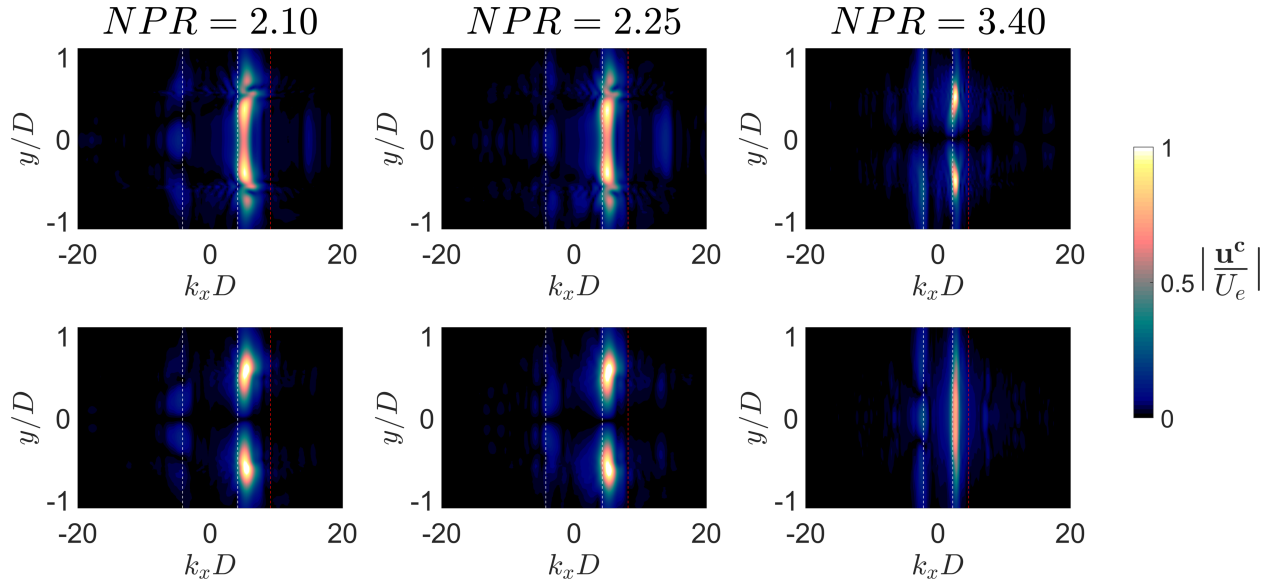


Figure 5. Wavenumber spectra for all three jets. Upper)  $u = u$ . Lower)  $u = v$

concentrated at a wavenumber associated with a phase velocity of  $u_p \approx 0.7U_j$ , with radial structures typical of the classical Kelvin-Helmholtz wavepacket. All three jets also have a component with an upstream phase velocity equal to the speed of sound, this is the signature of the neutrally-stable acoustic mode previously documented in screeching jets.<sup>13,14</sup> There is an additional “blob” of energy at high wavenumber, observed for all jets, though with different radial structure for the  $m = 1$  case compared to  $m = 0$ .

The standing wave set up between the downstream-propagating hydrodynamic waves and the upstream-propagating acoustic waves is well recognized as a source of spatial velocity modulation. To determine other sources of modulation, we remove the effects of the standing wave. This is achieved by removing all fluctuations with negative phase velocity via filtering in wavenumber space. The amplitudes calculated only from the fluctuations with positive phase velocity are plotted in Figures 6 and 7. The resultant plots of fluctuation amplitude exhibit markedly less spatial modulation; it is immediately apparent that the majority of spatial modulation outside the jet lipline ( $r/D = 0.5$ ) has been removed. Without the upstream-travelling acoustic waves, it appears that there is effectively no modulation of velocity taking place outside of the shear layer. Inside the jet however, significant modulation remains. For the toroidal screech cases, there is a periodic oscillation of axial velocity fluctuation amplitude associated with the shocks in the jet core, but relatively little modulation of the transverse velocity component. For the helical screech mode, there remains significant modulation of velocity in both the axial velocity (primarily on the high-speed side of the shear layer) and the transverse velocity (at the centreline).

In this paper we will afford little further consideration to fluctuations with negative phase velocity, and focus largely on the downstream-propagating components in an attempt to determine whether other mechanisms of spatial modulation are in effect. Firstly we return to the two discrete signatures with positive phase velocity identified in Figure 5: the Kelvin-Helmholtz wavepacket and the “blob”. We apply a Gaussian bandpass filter of  $\sigma = 1.5k_x D$  in the wavenumber domain, centred on the maximum amplitude within the local region for both the KH wave and the blob. The amplitude of the fluctuations resulting from this filtering is presented for  $NPR = 2.10$  in Figure 8 and for  $NPR = 3.40$  in Figure 9. The spatial distribution of the KH wavepacket closely resembles the distribution in Figures 6 & 7, absent any of the spatial modulation. This result is unsurprising; the majority of the downstream-propagating energy is associated with the KH wave, and the modulation in the original data cannot be represented with a narrow bandpass filter as used here. The distribution associated with the blob is somewhat different. For the  $NPR = 2.10$  case, there is almost no transverse fluctuation associated with the blob; the fluctuations are largely axial, confined within the shear layer of the jet, and strongest around  $x/D \approx 2.5$ . At  $NPR = 3.40$ , the axial and transverse fluctuations associated with the blob are of similar amplitude, but go to zero at the centreline for the axial, but reach a maximum at the centreline for the transverse. The axial fluctuations are strongest around  $x/D \approx 4$ , and

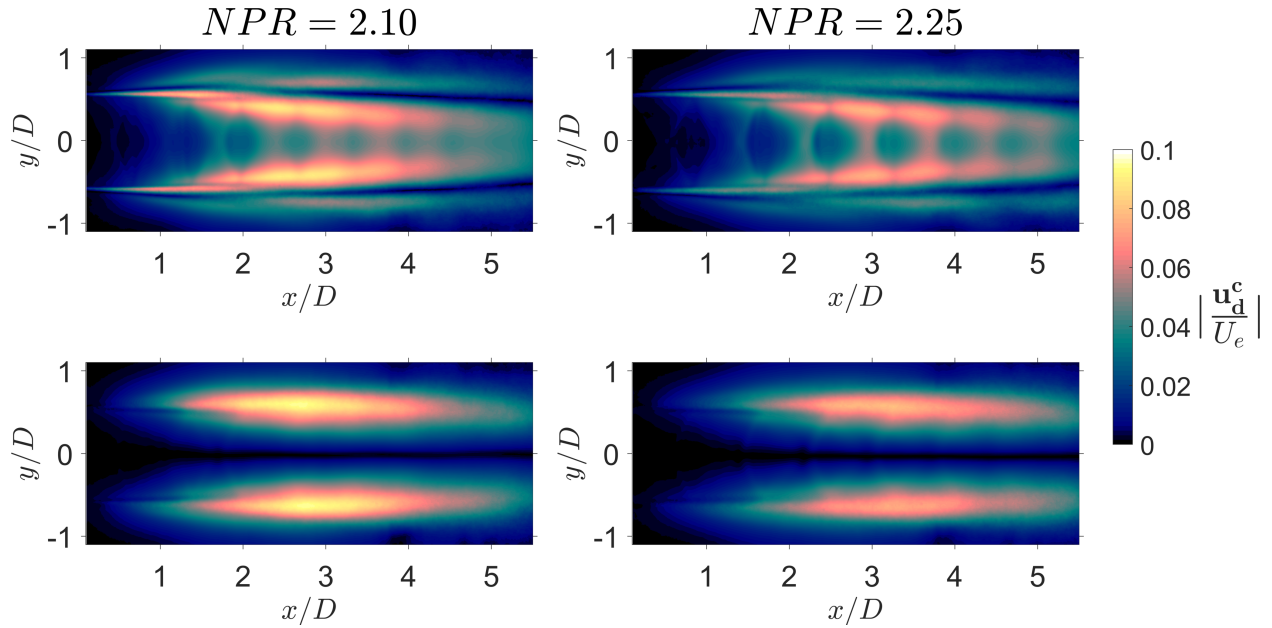


Figure 6. Magnitude of coherent fluctuations with positive phase velocity for the two jets where the screech mode is an  $m = 0$  azimuthal mode. Upper)  $u = u$ . Lower)  $u = v$ .

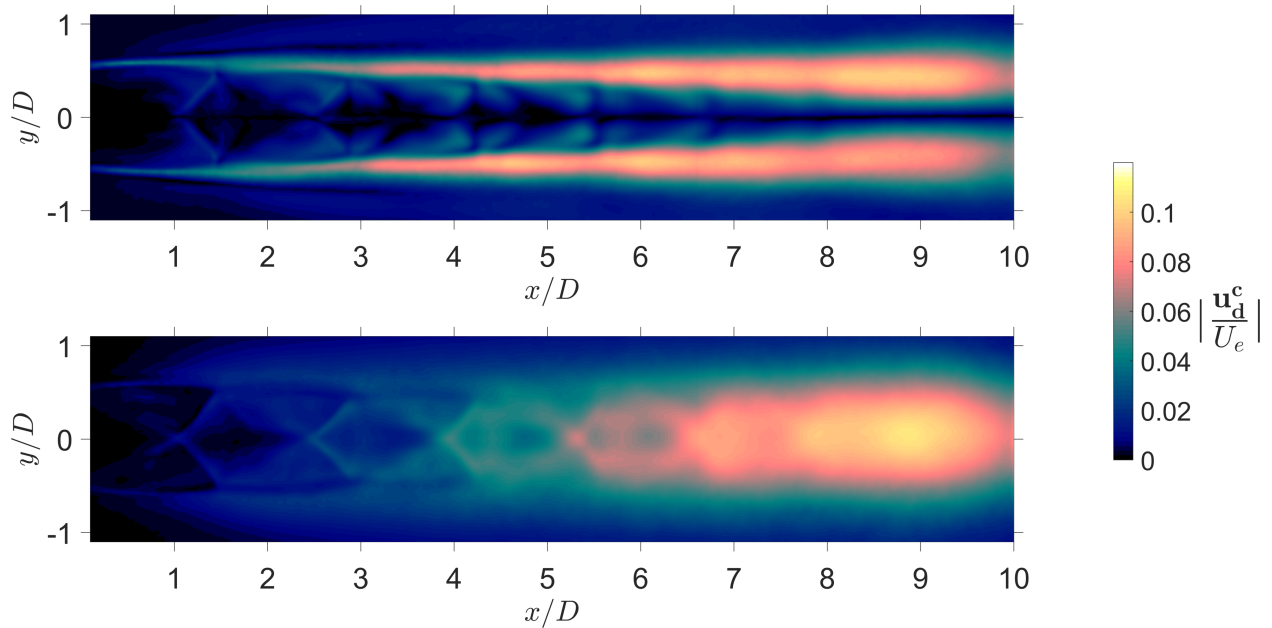


Figure 7. Magnitude of coherent fluctuations with positive phase velocity for jet where the screech mode is an  $m = 1$  azimuthal mode. Upper)  $u = u$ . Lower)  $u = v$ .

the transverse are strongest around  $x/D \approx 5$ . A consideration of Figures 1 and 2 suggests that the peak fluctuations for the blob occur around the location of the fourth shock cell for both cases. We now turn to our stability tools to further interrogate the behaviour of the KH wave and the nature of the 'blob'.

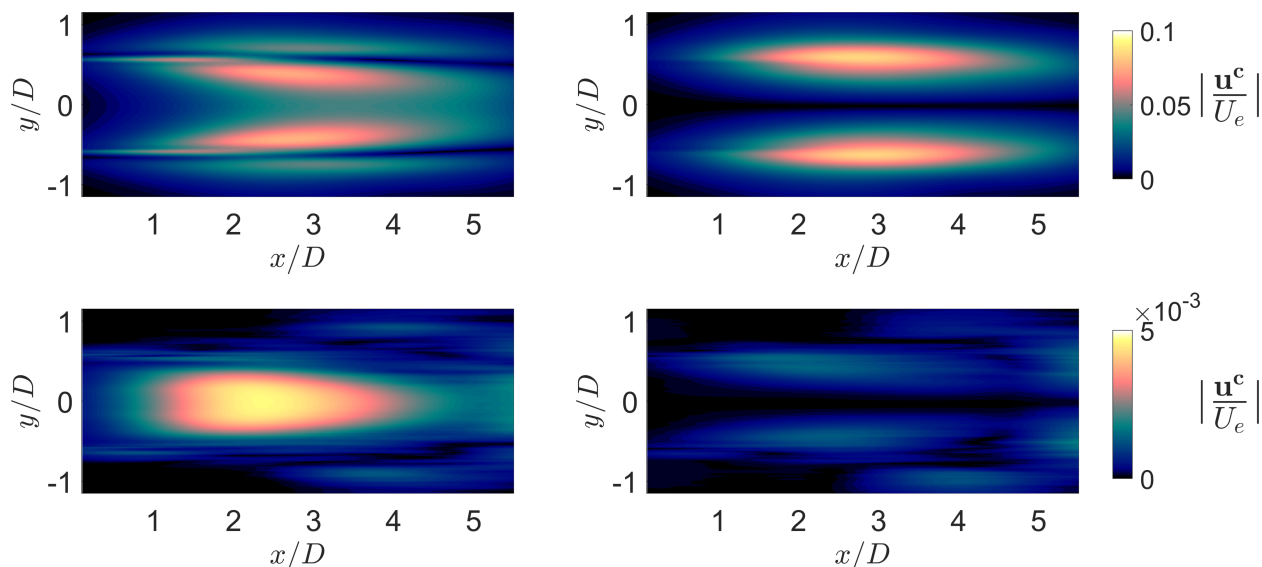


Figure 8. Magnitude of coherent fluctuations resulting from bandpass filtering for jets where the screech mode is an  $m = 0$  azimuthal mode. Left)  $u = u$ . Right)  $u = v$ . Upper) Filtering performed about KH mode. Lower) Filtering performed about 'blob'.

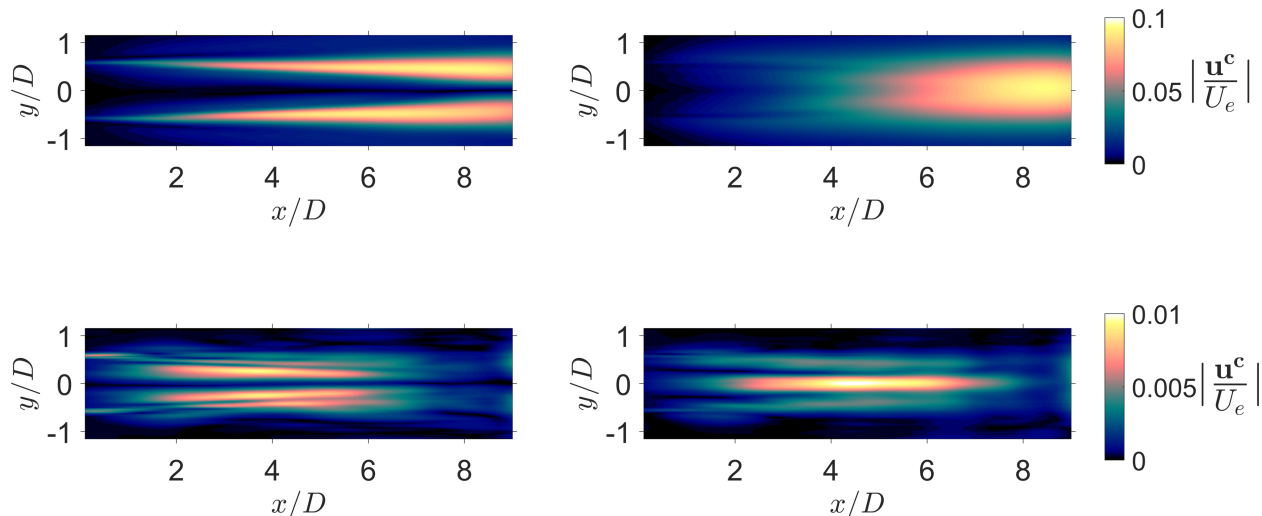


Figure 9. Magnitude of coherent fluctuations resulting from bandpass filtering for jet where the screech mode is an  $m = 1$  azimuthal mode. Left)  $u = u$ . Right)  $u = v$ . Upper) Filtering performed about KH mode. Lower) Filtering performed about 'blob'.

## B. Linear Stability Analysis

### 1. Global Analysis

We first consider a global analysis of the problem. Significant uncertainty remains regarding the effect of shocks and shock-like discontinuities on the validity of a linear stability analysis; we seek to ameliorate any such effects in two ways. Firstly, we consider only the  $NPR = 2.10$  case, where the shocks are extremely weak, and the transverse velocities are minimal. Much of the compression in a jet operating at this condition is achieved in a continuous fashion through near-isentropic compression waves. Additionally, the inability of

tracer particles to faithfully reproduce step changes in velocity is actually of benefit here; the discontinuities around shocks are inherently smoothed by our measurement technique. To enable the global analysis, the experimental domain is extrapolated to a field covering  $-1 \leq x/D \leq 15$  and  $0 \leq r/D \leq 4$ . Density information is not directly available from PIV, however by assuming that entropy generation by the weak shocks is negligible, an assumption of constant stagnation density along streamlines allows for a calculation of density from the velocity data. This is checked using a tomographic Background-Oriented-Schlieren measurement, with the axisymmetric field extracted from the path-integrated data using an Abel inversion;<sup>44</sup> errors due to the isentropic assumption appear to be less than 5%. The extrapolated fields are then divided into computational zones as per Figure 10. The core domain covers  $0 \leq x/D \leq 5$  and  $0 \leq r/D \leq 0.3$ , the shear layer zone covers  $0.3 \leq r/D \leq 0.7$ , and the far field extends to  $r/D = 3$ . Sponge layers are placed upstream and downstream of the jet, as well as outside the far field region.

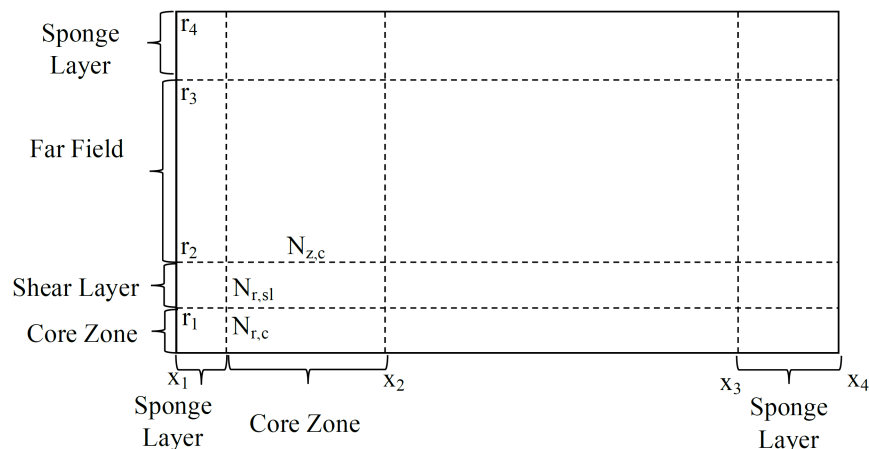


Figure 10. Calculation domain and mesh structure for the global analysis.

There are  $N_r = 300$  points in the radial direction: 100 in the core zone, 100 in the shear layer, and the rest shared between the far field and the sponge layer. To ensure mesh independence, two streamwise mesh discretizations are considered:  $N_x = 750$  and  $N_x = 1150$ . The eigenspectra for both streamwise discretizations are presented in Figure 11, calculated with a spacing in Frequency of  $\Delta St = 0.05$ . The overall trend in the continuous branch is reproduced between the two discretizations, while the modes closest to the real axis are very similar in both frequency and growth rate, suggesting the discretization is sufficient for our present purposes. Three modes of potential dynamical significance are observed, with the most relevant being the mode identified at  $St = 0.66$ , very close to the experimental value of  $St = 0.65$  for the screech tone observed for this jet. While the other two modes have interesting properties that may be of future interest, for the remainder of this work we will focus exclusively on the mode at  $St = 0.66$ , which notably is the least-damped mode.

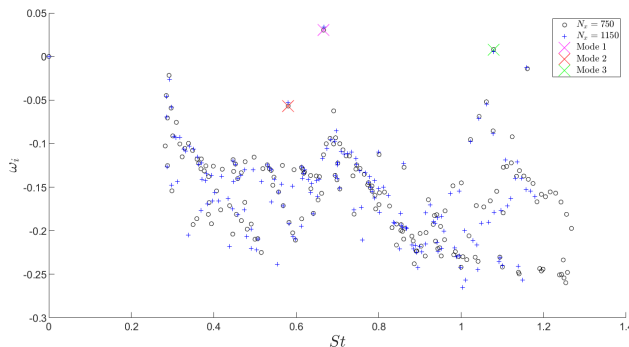
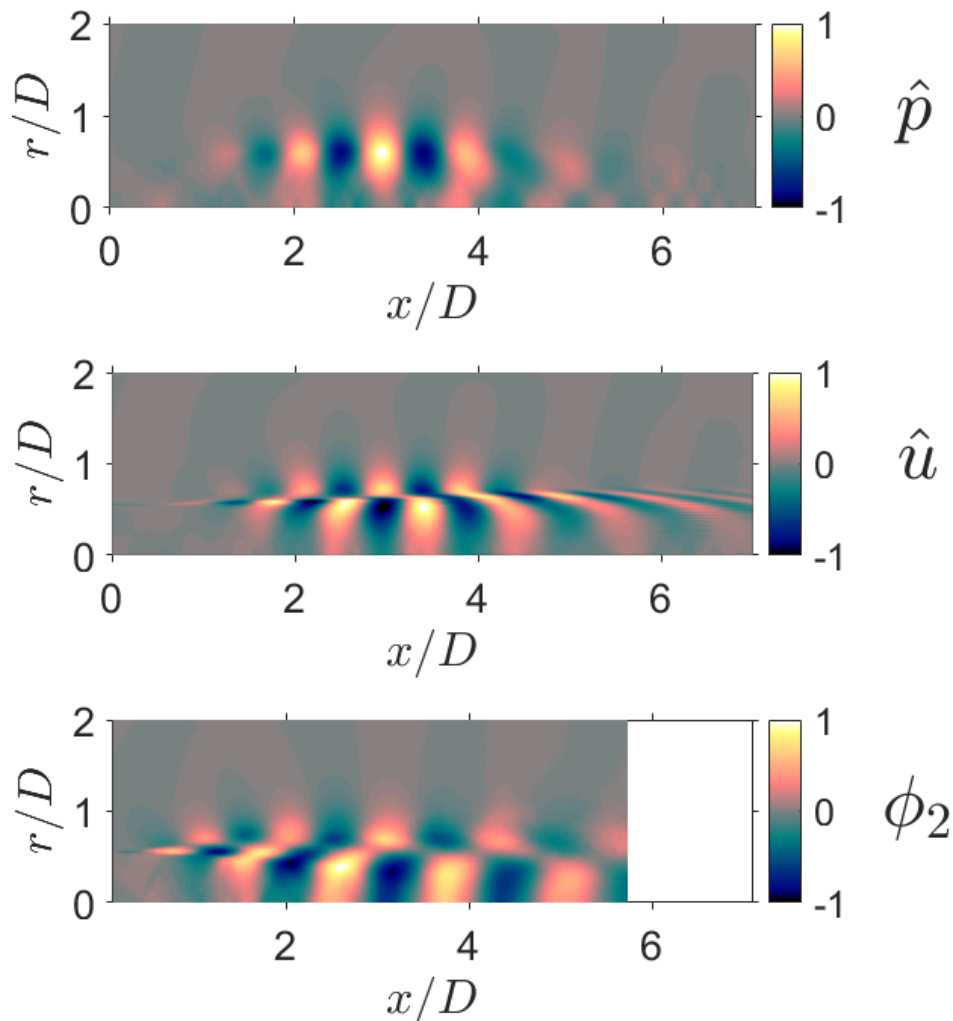


Figure 11. Eigenspectrum from global stability analysis for the  $NPR = 2.10$  jet.

We examine the spatial structure of this mode, presented in Figure 12, and present a comparison to

one of the leading POD modes extracted from the experimental data. A remarkable similarity between the experimental POD mode and the global mode is immediately apparent. While the streamwise velocities are not identical, given that the global mode was calculated from a linearization of an extrapolated base flow, the agreement is surprisingly good.



**Figure 12.** Pressure (upper) and streamwise velocity (middle) associated with the global mode identified at  $St = 0.66$ , presented with an experimentally determined POD streamwise velocity mode (bottom). All modes are normalized against their maximum value. All results for  $NPR = 2.10$  jet.

A further comparison is available in a consideration of the absolute value of the eigenmode with the fluctuations associated with the leading POD mode pair, as is demonstrated in Figure 13. Qualitatively, the two results are very similar. The streamwise velocity demonstrates modulation both in the jet core and outside the shear layer for both the global analysis and the experimental data. The transverse velocity is even more closely matched. There are however also some key differences; the magnitude of fluctuations in the jet core is much higher for the experimental data, and the modulation of these fluctuations is much stronger.

Performing a Fourier transform in the streamwise direction allows for a comparison of wavenumber spectra between the global analysis and the experimental decomposition. This comparison is presented in Figure 14; contour levels have been chosen to highlight structure other than the Kelvin-Helmholtz wave, which has by far the greatest amplitude. The spectra of the global mode is cleaner than that of the experimental data, but the same three structures visible in the experimental data are likewise visible: an upstream-propagating acoustic mode, a downstream-propagating Kelvin-Helmholtz wave, and the high wavenumber blob. Both the upstream mode and the blob are significantly stronger in the experimental data than in the global mode, though they are unequivocally evident in both. Both the KH wave and the blob are at a slightly higher

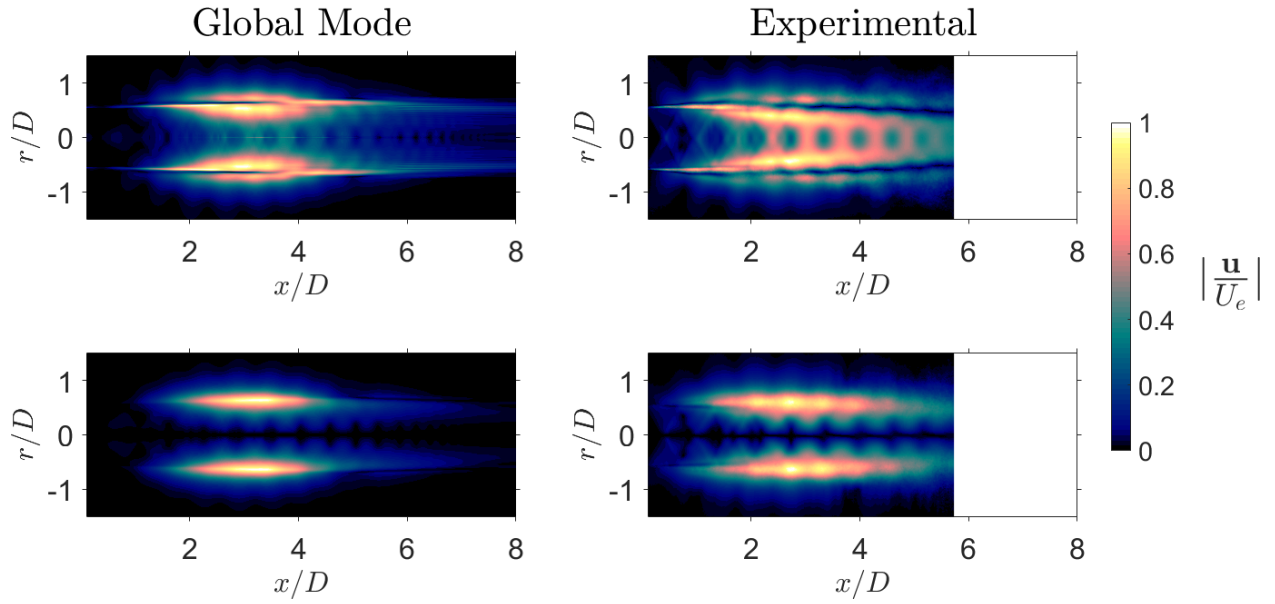


**Figure 13.** Magnitude of fluctuations from both experiment and global analysis. Upper)  $u = u$ . Lower)  $u = v$ . All results for  $NPR = 2.10$  jet.

wavenumber in the global analysis than the experimental data, while the upstream mode is essentially at the same wavenumber (corresponding to the speed of sound in the upstream direction).

A comparison of the radial profiles of streamwise velocity for the three identified structures, deduced from both experiment and stability analysis, are presented in Figure 15. All curves have been lightly smoothed with a moving average filter to reduce noise; no major features have been removed. The upstream mode has both the same wave number and a very similar radial structure, though the radial decay is slower for the global mode. The KH mode has a higher wavenumber for the global mode ( $k_x D = 7.0$ ) than for the experimentally-educed mode ( $k_x D = 5.5$ ), corresponding to phase velocities of  $u_p \approx 0.6$  and  $u_p \approx 0.75$  respectively. The radial structure for both experiment and LSA exhibits the characteristic double peak of a KH wavepacket, though the inner peak is shifted further from the jet centreline for the global mode. Finally, the peak wavenumber for the blob is once again slightly higher for the global mode ( $k_x D = 17.2$ ) than for the experimental result ( $k_x D = 14.9$ ). This offset is very similar to that observed for the KH mode (within the wavenumber resolution limit of the experimental decomposition, it is the same), a point we will return to in a later section. The radial structure of the blob mode is very similar for the two analyses, though there is a small peak at  $r/D \approx 0.5$  for the global mode that is not reproduced in the experiment.

The global analysis has done a remarkable job of capturing the same key structures observed in experiment. Given the assumptions made in both the experiment (that the key dynamics are captured by the leading POD mode pair) and the global analysis (that the problem can be viewed in a linear framework), this is a reassuring result. The global analysis predicts streamwise modulation of the fluctuations, though the modulation is weaker than that observed in experiment. Whether this modulation is a result of changes to the KH wavepacket or the interaction of multiple waves within the flow remains an open question. To shed some further light, we turn to a local analysis.

## 2. Local Analysis

Apart from the reduction in computational time, the local analysis can reveal mechanisms not immediately obvious in the global analysis, precisely because it does not include the entire domain. An exemplar eigenspectrum (taken at the nozzle exit plane  $x/D = 0$ ) is presented in Figure 16. Eigenvalues thought to be associated with the three modes identified in the global analysis and in the experimental data are indicated in the figure. Here a mode with positive phase-velocity is identified as a “trapped” mode;<sup>45</sup> this nomenclature will be discussed further in the following section. The eigenspectra evolves as a function of axial position, as the radial structure of the meanflow likewise evolves. These results will be used in the next section to inform both the behaviour of the KH wavepacket, and say something about the nature of the ‘blob’.

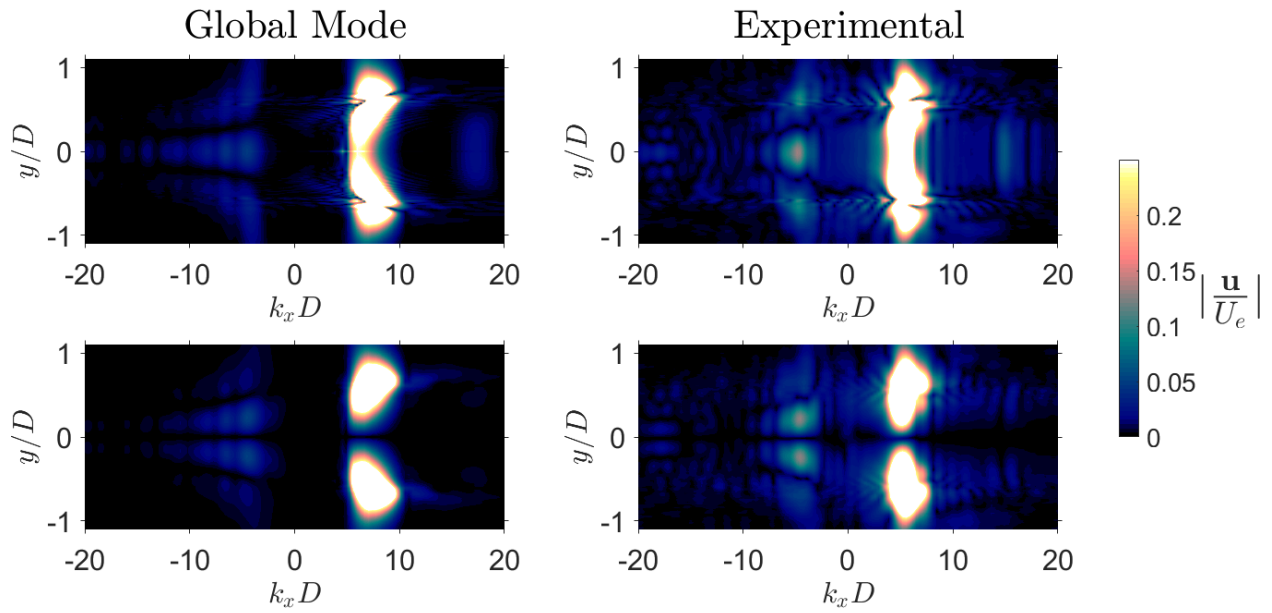


Figure 14. Wavenumber spectra from both global mode and experiment. Upper)  $u = u$ . Lower)  $u = v$ . All results for  $NPR = 2.10$  jet.

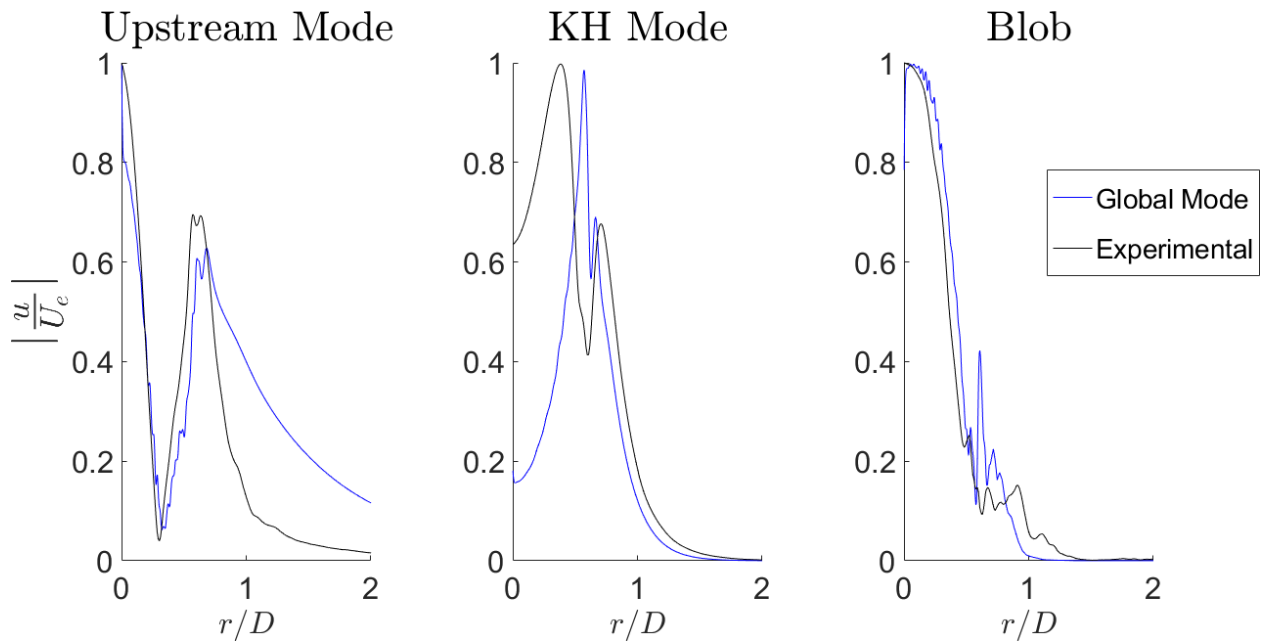


Figure 15. Radial profiles of streamwise velocity for the three modes discussed in this paper. All modes are normalized to their own maximum value. All results for  $NPR = 2.10$  jet.

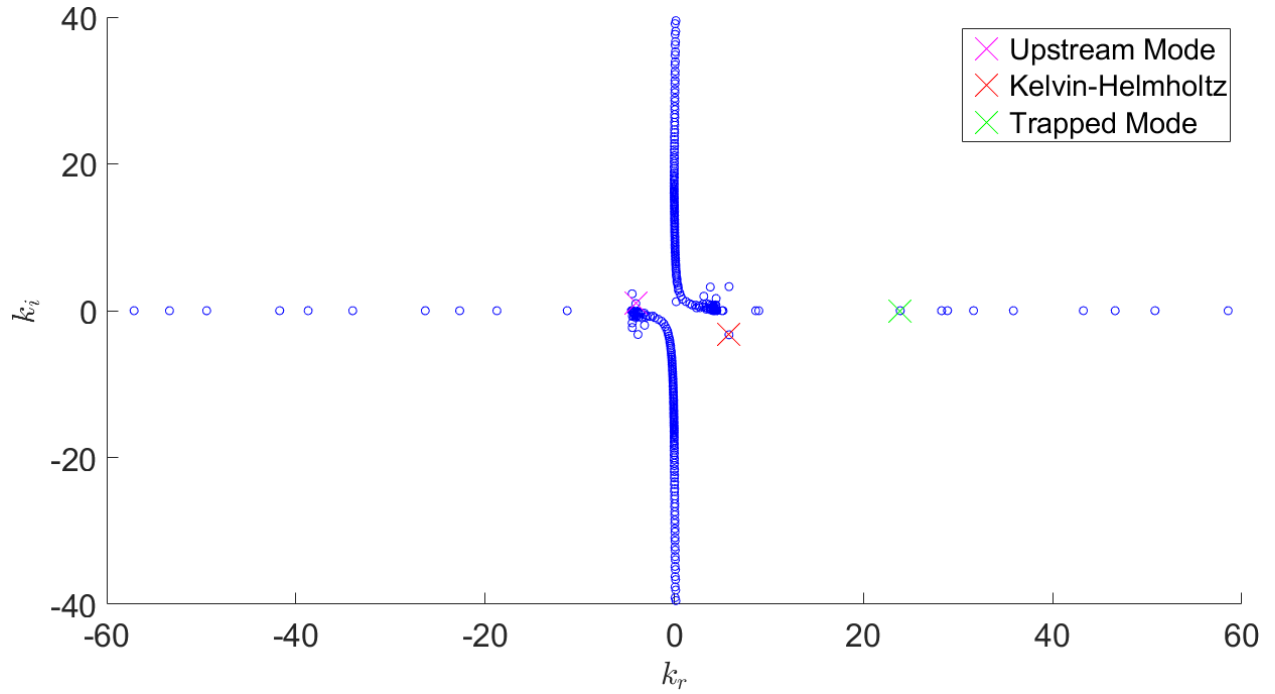


Figure 16. Eigenspectrum for local stability analysis, based on velocity profile extracted at  $x/D = 0$ .

## V. Discussion

The motivating question of this paper concerned the modulation of the KH wavepacket; do either the shocks or the resonance influence the spatial growth of this structure? The experimental decomposition makes it reasonably clear that while the upstream-propagating waves produce a strong standing wave in the hydrodynamic nearfield, for the flows considered here, there is little evidence that the downstream wave is itself altered by this interaction; the resulting fluctuations appear to be a simple linear superposition of the upstream and downstream waves. Whether the shocks act to modulate the KH wave is less clear from the analysis presented thus far. There are (at least) two mechanisms by which the shocks could affect the growth of the KH wavepacket: a direct non-linear interaction between the shock and the wavepacket, or changes in the growth of the wavepacket due to changes in the base flow driven by the presence of shock and expansion waves. The second mechanism here is ideal for interrogation by the local linear analysis. By extracting the spatial growth rates associated with the Kelvin-Helmholtz mode as a function of streamwise position, the local analysis can determine whether variations in the base flow drive modulations of the wavepacket. Figure 17 provides a centreline profile of  $u^c u^c$  extracted from the experimental data, for both total fluctuations, and for fluctuations resulting from the bandpass filter around the KH peak wavenumber discussed earlier. The fluctuations are clearly oscillations around the underlying growth of the KH wavepacket; a moving average filter applied to the data would achieve much the same result as the filtering in wavenumber space. Also provided in the figure is the normalized growth rate of the KH wave as a function of streamwise position, determined by the local linear stability analysis. The modulation observed in the total fluctuations is not observed in the local analysis; there is no modulation of the growth rate matching the length-scales of the shock structures as is evident in the experimental data. The local analysis predicts the KH wavepacket to saturate slightly earlier ( $x/D \approx 2$ ) than observed in experiment ( $x/D \approx 3$ ). Nonetheless, at this frequency, and for these shock structures, the LSA clearly demonstrates that the growth rate of the KH wavepacket is relatively insensitive to the variations in the base flow induced by the shocks; the thickening of the shear layer with increasing axial position is clearly a far stronger effect than anything related to the shocks.

If the local analysis is suggesting that changes in the base flow are insufficient to produce the modulations observed in the downstream-propagating components of the flow, then the source of these modulations remains to be established. We consider interaction between the three wave moving wavelike structures in the flow, as well as the stationary wave structure of the shocks. This is achieved via the application of

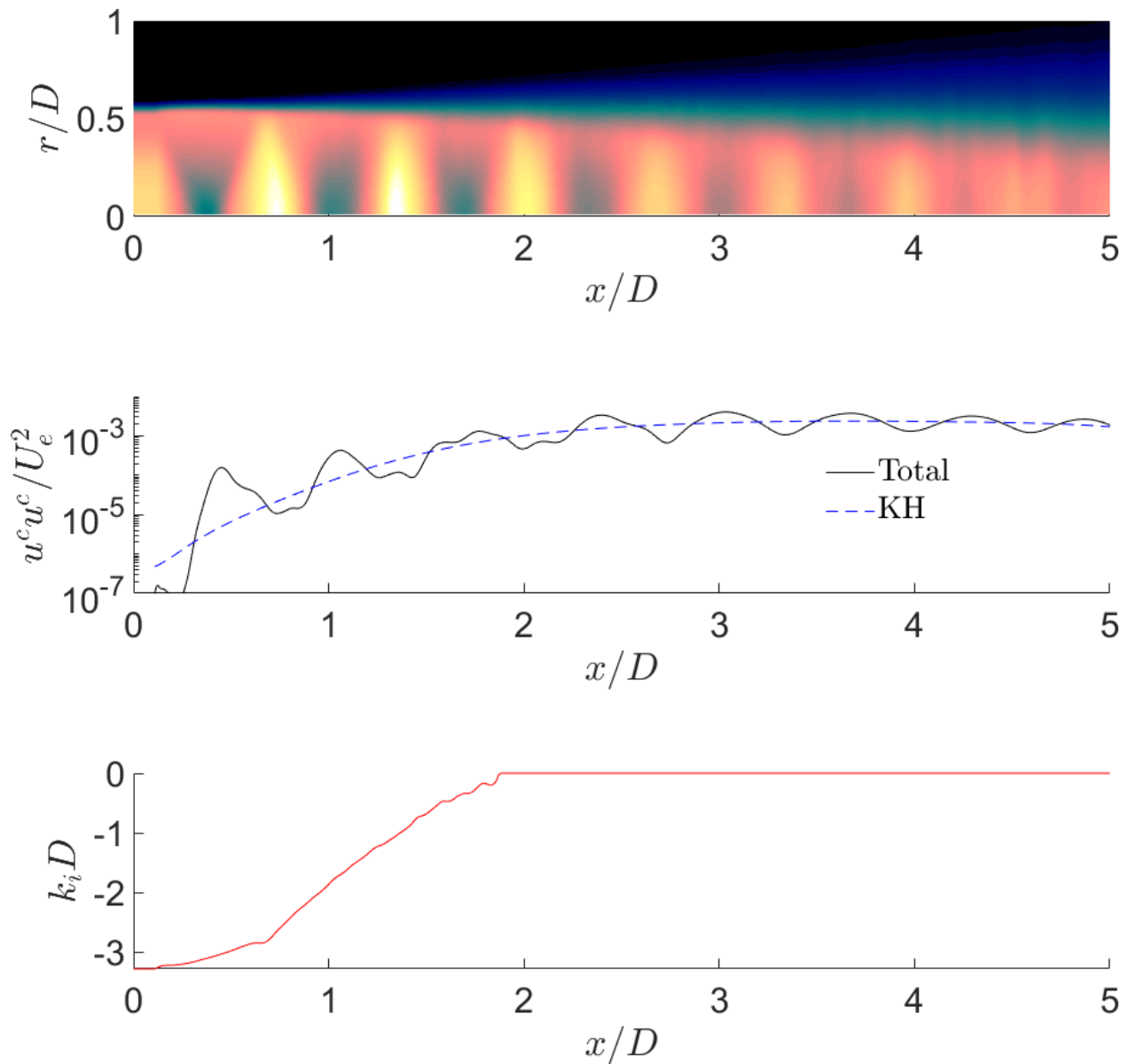
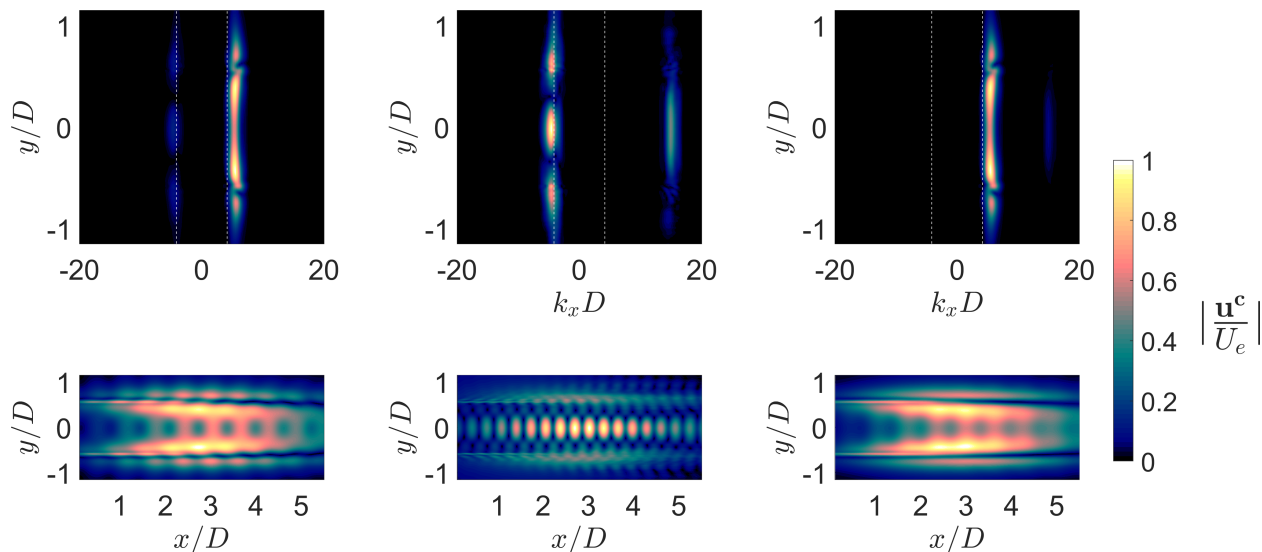


Figure 17. Upper) Time-averaged density field educed from experiment. Middle) Centreline velocity fluctuations from experiment, with and without bandpass filtering around the KH wavenumber. Bottom) Variation in spatial growth rate for the KH wavepacket, calculated from the local stability analysis. All results for  $NPR = 2.10$  jet.

dual-peaked bandpass filters in wavenumber space; the filtered wavenumber spectra are visible along with the resulting amplitude distributions in Figure 18. The combination of the downstream-propagating KH wave and the upstream-propagating acoustic mode is sufficient to produce an amplitude pattern remarkably similar to that of the full field. This reinforces what was observed in Figure 6, where much of the modulation (but not all) was removed with the filtering out of the upstream-propagating acoustic mode. Interaction between the upstream mode and the blob mode produces a strongly modulated pattern of fluctuations in the core of the jet, but these are at a much higher wavenumber than the modulation observed in the total fluctuations. Lastly, a combination of the blob and the KH mode is considered, and this returns fluctuations at the same wavelength as the combination of KH + upstream mode, though only in the core of the jet. Thus the modulation of velocity fluctuation in the shear layer can be seen to be driven purely by an interaction between the KH wavepacket and the upstream acoustic mode, while the modulation of fluctuations in the jet core is from the interaction of the KH wave with both the upstream acoustic mode and the blob mode.



**Figure 18.** Interaction between pairs of modes for  $NPR = 2.10$  jet, represented through streamwise velocity fluctuations ( $u = u$ ). Top) Wavenumber spectra. Bottom) Velocity fluctuation amplitude (normalized)

The relative influence of the two interactions is displayed in Figure 19. It is clear that the downstream/upstream interaction is responsible for more of the centreline modulation, but that the downstream/downstream contribution is non-trivial between the second and fifth shock cells.

The helical  $m = 1$  jet at  $NPR = 3.40$  is also considered, with similar findings. Outside of the shear layer all the modulation can be explained by the interaction of the KH mode with the upstream-propagating wave. Within the core of the jet however, the situation is rather more complex. There is streamwise modulation by both interactions, however the distribution of the modulation pattern is quite different. The interaction with the upstream mode produces a modulation pattern where lobes of fluctuation move towards the centreline at an angle towards the upstream direction. Conversely, the interaction between the two downstream-propagating waves produces lobes that move towards the centreline at an angle towards the downstream direction.

Figure 19 appears to indicate that the modulation of velocity fluctuations is occurring approximately at the spacing of the shocks. The shocks are of course inextricably linked to the screech cycle, given that it is thought to be the interaction of the KH wavepacket with the shocks that produces the upstream wave. To further discern the relationship between the shocks and these other three wavestructures, the peak wavenumbers of all three waves, as well as the wavenumber of the stationary shock system, are presented in Table 3. It is important to note that these are only peak values, and the energy for all modes is spread around this wavenumber. Given that the spatial modulation could be represented as a beating between waves of different wavenumber, Table 4 presents the difference between the wavenumbers of the KH, Blob and upstream acoustic modes. When interpreting these results, keep in mind that the spatial resolution is approximately  $0.3D$ , that these are only peak values with a spread of wavenumbers around them, and that shock spacing varies somewhat over the length of the domain. Given the aforementioned points there is a

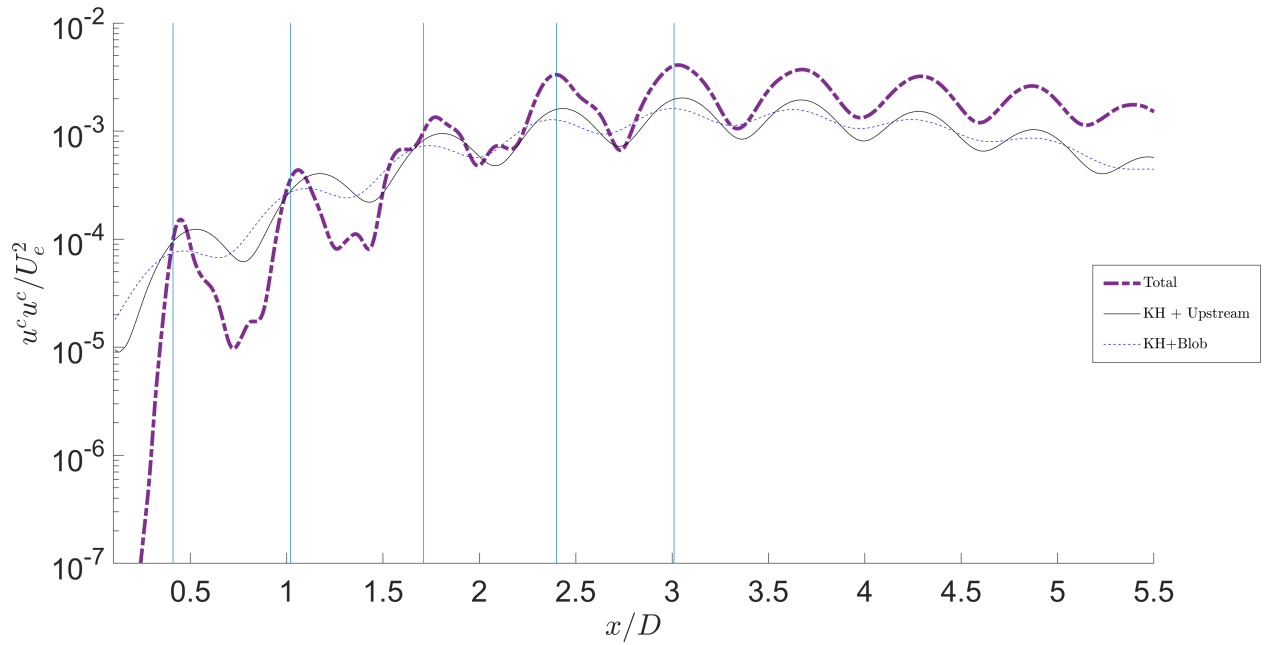


Figure 19. Centreline streamwise velocity fluctuations: total, KH+Upstream, KH+Blob, for  $NPR = 2.10$  jet. Top) Wavenumber spectra. Vertical lines indicate centreline shock positions.

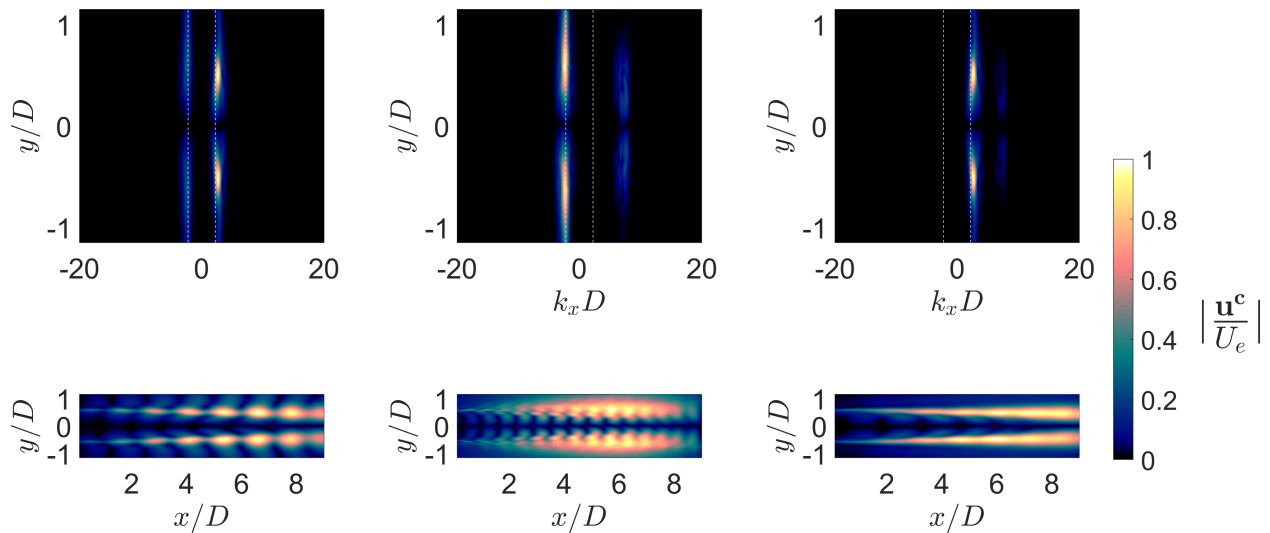


Figure 20. Interaction between pairs of modes for  $NPR = 3.40$  jet, represented through streamwise velocity fluctuations ( $u = u$ . Top) Wavenumber spectra. Bottom) Velocity fluctuation amplitude (normalized)

clear match between the beat wavenumbers ( $\Delta k_x$ ) between the KH wavepacket and both the upstream and downstream modes, and this wavenumber also matches the shock spacing.

This result for the upstream wave is intuitive, if one considers the general assumption that screech tones (and thus the upstream wave at the screech frequency) are produced by an interaction between the KH wavepacket and the shocks within the flow. This result reinforces the spacing of the shocks as a critical lengthscale of the flow; there is currently some debate as to whether screech originates from a single source or multiple sources.<sup>46</sup> This does not close that debate, but the data here fits the picture of an upstream wave produced by an interaction between the KH wave and a stationary wavelike structure in the form of a series of shocks.

The beat wavenumber between the two downstream-propagating waves also matches the shock spacing to within the experimental uncertainty for all cases considered. At this point it seems clear, that much like the neutral upstream acoustic mode, the 'blob' is generated by the interaction of the KH wavepacket with the stationary shock structures within the flow. This is consistent with the spatial amplitude variation observed in Figure 8; the blob is strongest where the interaction between the KH wave and the shocks is strongest (this location is consistent with the peaks observed in the spatial distribution of the upstream mode as well). As is demonstrated in Figure 15 however, the radial structure of the blob is distinctly different to that of the upstream-propagating acoustic mode.

**Table 3. Wavenumbers of wave structures**

NPR	$k_x D(KH)$	$k_x D(Blob)$	$k_x D(Acoustic)$	$k_x D(Shocks)$
2.10 (Exp)	5.2	14.9	-4.6	9 - 10.5
2.10 (LSA)	7.0	17.2	-4.2	9 - 10.5
2.25	4.9	13.6	-3.6	7.4 - 8.6
3.4	2.8	7.4	-2.1	4.3 - 4.6

**Table 4. Wavenumber differences**

NPR	$\Delta k_x D(KH - Blob)$	$\Delta k_x D(KH - Acoustic)$	$k_x D(Shocks)$
2.10 (Exp)	9.7	9.8	9 - 10.5
2.10 (LSA)	9.9	11.2	9 - 10.5
2.25	8.7	8.5	7.4 - 8.6
3.4	4.6	4.9	4.3 - 4.6

What is the nature of this downstream-propagating interaction wave, and what relationship does it have to the base flow of the jet? One clear candidate to explain this wave is the subsonic instability modes first identified in Tam and Hu,<sup>10</sup> and recently demonstrated to form components of resonance in subsonic jets.<sup>15, 45, 47</sup> These waves are confined to the interior of the jet, and are acoustic modes that essentially treat the boundaries of the jet like a soft-walled duct. The radial structure of these trapped waves is qualitatively similar to that observed in Figure 15, but this alone may be considered insufficient evidence. Considering the local stability analysis, the duct-like "trapped" mode is identifiable in the eigenspectra (Figure 16) for the flow at  $x/D = 0$ . Here however the wavenumber is  $k_x D \approx 24$ , significantly higher than the wavenumber of the blob observed in either experiment or the global analysis. Moving only a short distance downstream however, to an axial station at  $x/D = 1.05$ , the wavenumber of the trapped mode has already reduced to  $k_x D \approx 16$ , comparable to the value observed both in experiment and the global analysis. Thus the local analysis is demonstrating that the base flow is capable of supporting a trapped wave at this combination of frequency and wavenumber. The next point of inquiry is whether the radial structure of the trapped wave matches that of the blob. This is examined in Figure 21. Two streamwise stations are considered for the radial profile used for the local analysis. Picking the profile at  $x/D = 1.5$  produces a profile that very closely matches the experimental signature of the blob, at least until the lipline. This result is however highly sensitive to the choice of radial profile; moving the streamwise position to  $x/D = 2.5$ , close to the peak amplitude of the trapped wave, produces a poorer result, though the qualitative structure is certainly

preserved. On the basis of the available evidence it cannot be established beyond doubt that the blob is indeed a duct-like trapped mode, however the agreement certainly suggests that possibility. This will be a topic of further investigations.

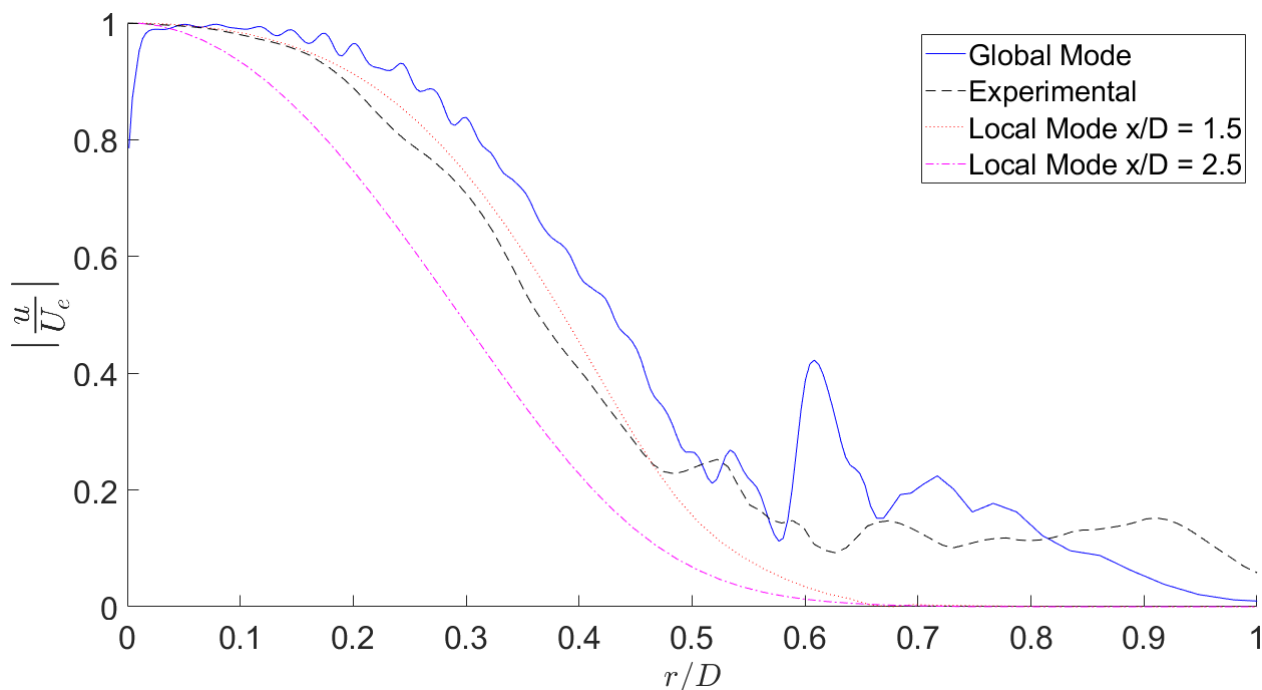


Figure 21. Radial streamwise velocity profiles for the 'blob' mode, from experiment, from global analysis, and from local analysis at two streamwise positions. Results for  $NPR = 2.10$  jet.

## VI. Conclusion

This paper set out to determine the source of spatial modulation of velocity in shock-containing resonant jets. The investigation constituted both decomposition of experimental data and the application of a hierarchy of stability tools. On the basis of these analyses, the following statements can be made:

- There are three distinct wavelike structures present in screeching jets; one upstream-propagating wave and two downstream-propagating waves. The upstream mode is the previously-identified neutral acoustic mode. One of the downstream modes is the well-recognized Kelvin-Helmholtz wavepacket. The other appears to be a trapped duct-like acoustic mode with positive phase velocity, though this awaits final confirmation.
- It is the interaction of the KH wavepacket with the stationary shocks in the jet that selects the wavenumber for both the upstream-propagating acoustic wave and the downstream-propagating duct-like wave.
- The superposition of these three wavelike structures is sufficient to explain almost all the spatial modulation of velocity observed in these jets.
- Outside the shear layer, almost all the modulation is driven by interaction between the upstream-propagating acoustic mode and the downstream-propagating Kelvin-Helmholtz wavepacket.
- Within the shear layer, the modulation results from both the aforementioned interaction, as well as an interaction between the KH wavepacket and the trapped mode.
- The evidence suggests that the growth of the KH wavepacket is relatively insensitive to the shocks; it interacts with the shocks and produces two new waves as a result, but its own growth is unaffected by this interaction (at least for weak shocks).

## References

- <sup>1</sup>Edgington-Mitchell, D., “Aeroacoustic resonance and self-excitation in screeching and impinging supersonic jets—A review,” *International Journal of Aeroacoustics*, 2019, pp. 1475472X19834521.
- <sup>2</sup>Tam, C. K. and Ahuja, K., “Theoretical model of discrete tone generation by impinging jets,” *Journal of Fluid Mechanics*, Vol. 214, 1990, pp. 67–87.
- <sup>3</sup>Gudmundsson, K. and Colonius, T., “Instability wave models for the near-field fluctuations of turbulent jets,” *Journal of Fluid Mechanics*, Vol. 689, 2011, pp. 97–128.
- <sup>4</sup>Sinha, A., Rodríguez, D., Brès, G. A., and Colonius, T., “Wavepacket models for supersonic jet noise,” *Journal of Fluid Mechanics*, Vol. 742, 2014, pp. 71–95.
- <sup>5</sup>Manning, T. and Lele, S., “A numerical investigation of sound generation in supersonic jet screech,” *21st AIAA Aeroacoustics Conference*, 2000.
- <sup>6</sup>Suzuki, T. and Lele, S. K., “Shock leakage through an unsteady vortex-laden mixing layer: application to jet screech,” *Journal of Fluid Mechanics*, Vol. 490, 2003, pp. 139–167.
- <sup>7</sup>Shariff, K. and Manning, T. A., “A ray tracing study of shock leakage in a model supersonic jet,” *Physics of Fluids (1994-present)*, Vol. 25, No. 7, 2013, pp. 076103.
- <sup>8</sup>Berland, J., Bogey, C., and Bailly, C., “Numerical study of screech generation in a planar supersonic jet,” *Phys. Fluids*, Vol. 19, 2007.
- <sup>9</sup>Edgington-Mitchell, D. M., Weightman, J. L., Honnery, D. R., and Soria, J., “Sound production by shock leakage in supersonic jet screech,” *2018 AIAA/CEAS aeroacoustics conference*, 2018, p. 3147.
- <sup>10</sup>Tam, C. and Hu, F., “On the three families of instability waves of high-speed jets,” *J. Fluid Mech.*, Vol. 201, 1989, pp. 447–483.
- <sup>11</sup>Shen, H. and Tam, C., “Three-Dimensional Numerical Simulation of the Jet Screech Phenomenon,” *AIAA J.*, Vol. 40, 2002, pp. 33–41.
- <sup>12</sup>Bogey, C. and Gojon, R., “Feedback loop and upwind-propagating waves in ideally expanded supersonic impinging round jets,” *Journal of Fluid Mechanics*, Vol. 823, 2017, pp. 562–591.
- <sup>13</sup>Gojon, R., Bogey, C., and Mihaescu, M., “Oscillation Modes in Screeching Jets,” *AIAA Journal*, 2018, pp. 1–7.
- <sup>14</sup>Edgington-Mitchell, D., Jaunet, V., Jordan, P., Towne, A., Soria, J., and Honnery, D., “Upstream-travelling acoustic jet modes as a closure mechanism for screech,” *Journal of Fluid Mechanics*, Vol. 855, 2018.
- <sup>15</sup>Jordan, P., Jaunet, V., Towne, A., Cavalieri, A. V., Colonius, T., Schmidt, O., and Agarwal, A., “Jet–flap interaction tones,” *Journal of Fluid Mechanics*, Vol. 853, 2018, pp. 333–358.
- <sup>16</sup>Barone, M. F. and Lele, S. K., “Receptivity of the compressible mixing layer,” *Journal of Fluid Mechanics*, Vol. 540, 2005, pp. 301–335.
- <sup>17</sup>Mitchell, D. M., Honnery, D. R., and Soria, J., “The visualization of the acoustic feedback loop in impinging underexpanded supersonic jet flows using ultra-high frame rate schlieren,” *Journal of visualization*, Vol. 15, No. 4, 2012, pp. 333–341.
- <sup>18</sup>Weightman, J. L., Amili, O., Honnery, D., Edgington-Mitchell, D., and Soria, J., “Nozzle external geometry as a boundary condition for the azimuthal mode selection in an impinging underexpanded jet,” *Journal of Fluid Mechanics*, Vol. 862, 2019, pp. 421–448.
- <sup>19</sup>Powell, A., “On the mechanism of choked jet noise,” *Proc. Phys. Soc. London*, Vol. 66, 1953, pp. 1039–1056.
- <sup>20</sup>Michalke, A., “Survey on jet instability theory,” *Progress in Aerospace Sciences*, Vol. 21, 1984, pp. 159–199.
- <sup>21</sup>Morris, P. J., “The instability of high speed jets,” *International Journal of Aeroacoustics*, Vol. 9, No. 1, 2010, pp. 1–50.
- <sup>22</sup>Cavalieri, A. V., Rodríguez, D., Jordan, P., Colonius, T., and Gervais, Y., “Wavepackets in the velocity field of turbulent jets,” *Journal of fluid mechanics*, Vol. 730, 2013, pp. 559–592.
- <sup>23</sup>Ducros, F., Ferrand, V., Nicoud, F., Weber, C., Darracq, D., Gacherieu, C., and Poinot, T., “Large-eddy simulation of the shock/turbulence interaction,” *Journal of Computational Physics*, Vol. 152, No. 2, 1999, pp. 517–549.
- <sup>24</sup>Edgington-Mitchell, D., Stegeman, P., Kitsios, V., Honnery, D., Ooi, A., and Soria, J., “Reynolds stress anisotropy in shock containing jets,” *Turbulent Shear Flow Phenomenon*, Vol. 9, 2015.
- <sup>25</sup>Westley, R. and Woolley, J., “The near field sound pressures of a choked jet when oscillating in the spinning mode,” *2nd Aeroacoustics Conference*, 1975, p. 479.
- <sup>26</sup>Panda, J., “An experimental investigation of screech noise generation,” *J. Fluid Mech.*, Vol. 378, 1999, pp. 71–96.
- <sup>27</sup>Edgington-Mitchell, D., Oberleithner, K., Honnery, D. R., and Soria, J., “Coherent structure and sound production in the helical mode of a screeching axisymmetric jet,” *Journal of Fluid Mechanics*, Vol. 748, 2014, pp. 822–847.
- <sup>28</sup>Tan, D., Soria, J., Honnery, D., and Edgington-Mitchell, D., “Novel Method for Investigating Broadband Velocity Fluctuations in Axisymmetric Screeching Jets,” *AIAA Journal*, 2017, pp. 1–14.
- <sup>29</sup>Agui, J. and Jimenez, J., “On the performance of particle tracking,” *J. Fluid Mech.*, Vol. 185, 1974, pp. 447–468.
- <sup>30</sup>Mitchell, D. M., Honnery, D. R., and Soria, J., “Near-field structure of underexpanded elliptic jets,” *Experiments in fluids*, Vol. 54, No. 7, 2013, pp. 1578.
- <sup>31</sup>Jaunet, V., Jordan, P., and Cavalieri, A., “Two-point coherence of wave packets in turbulent jets,” *Physical Review Fluids*, Vol. 2, No. 2, 2017, pp. 024604.
- <sup>32</sup>Towne, A., Schmidt, O. T., and Colonius, T., “Spectral proper orthogonal decomposition and its relationship to dynamic mode decomposition and resolvent analysis,” *J. Fluid Mech.*, Vol. 847, 2018, pp. 821–867.
- <sup>33</sup>Schmidt, O. T., Towne, A., Rigas, G., Colonius, T., and Brès, G. A., “Spectral analysis of jet turbulence,” *J. Fluid Mech.*, Vol. 855, 2018, pp. 953–982.
- <sup>34</sup>Taira, K., Brunton, S. L., Dawson, S. T., Rowley, C. W., Colonius, T., McKeon, B. J., Schmidt, O. T., Gordeyev, S., Theofilis, V., and Ukeiley, L. S., “Modal analysis of fluid flows: An overview,” *AIAA Journal*, 2017, pp. 1–29.

- <sup>35</sup>Berkooz, G., Holmes, P., and Lumley, J., “The Proper Orthogonal Decomposition in the Analysis of Turbulent Flows,” *Annu. Rev. Fluid Mech.*, Vol. 25, 1993, pp. 539–575.
- <sup>36</sup>Sirovich, L., “Turbulence and the dynamics of coherent structures. I. Coherent structures,” *Quarterly of applied mathematics*, Vol. 45, No. 3, 1987, pp. 561–571.
- <sup>37</sup>Edgington-Mitchell, D., Honnery, D. R., and Soria, J., “The underexpanded jet Mach disk and its associated shear layer,” *Physics of Fluids*, Vol. 26, No. 9, 2014, pp. 096101.
- <sup>38</sup>Jaunet, V., Collin, E., and Delville, J., “POD-Galerkin advection model for convective flow: application to a flapping rectangular supersonic jet,” *Experiments in Fluids*, Vol. 57, No. 5, 2016, pp. 84.
- <sup>39</sup>Edgington-Mitchell, D., Honnery, D. R., and Soria, J., “Instability modes in screeching elliptical jets,” *20th AIAA/CEAS Aeroacoustics Conference*, 2014.
- <sup>40</sup>Edgington-Mitchell, D., Honnery, D. R., and Soria, J., “Multimodal Instability in the Weakly Underexpanded Elliptic Jet,” *AIAA Journal*, 2015, pp. 1–11.
- <sup>41</sup>Weightman, J. L., Amili, O., Honnery, D., Soria, J., and Edgington-Mitchell, D., “An explanation for the phase lag in supersonic jet impingement,” *Journal of Fluid Mechanics*, Vol. 815, 2017.
- <sup>42</sup>Oberleithner, K., Sieber, M., Nayeri, C., Paschereit, C., Petz, C., Hege, H.-C., Noack, B., and Wagnanski, I., “Three-dimensional coherent structures in a swirling jet undergoing vortex breakdown: stability analysis and empirical mode construction,” *Journal of Fluid Mechanics*, Vol. 679, 2011, pp. 383–414.
- <sup>43</sup>Towne, A. S., *Advancements in jet turbulence and noise modeling: accurate one-way solutions and empirical evaluation of the nonlinear forcing of wavepackets*, Ph.D. thesis, California Institute of Technology, 2016.
- <sup>44</sup>Tan, D. J., Edgington-Mitchell, D., and Honnery, D., “Measurement of density in axisymmetric jets using a novel background-oriented schlieren (BOS) technique,” *Experiments in Fluids*, Vol. 56, No. 11, 2015, pp. 204.
- <sup>45</sup>Towne, A., Cavalieri, A. V. G., Jordan, P., Colonius, T., Schmidt, O., Jaunet, V., and Brès, G., “Acoustic resonance in the potential core of subsonic jets,” *Journal of Fluid Mechanics*, Vol. 825, 2017.
- <sup>46</sup>Mercier, B., Castelain, T., and Bailly, C., “Experimental characterisation of the screech feedback loop in underexpanded round jets,” *Journal of Fluid Mechanics*, Vol. 824, 2017, pp. 202–229.
- <sup>47</sup>Towne, A., Schmidt, O. T., and Brès, G. A., “An investigation of the Mach number dependence of trapped acoustic waves in turbulent jets,” *25th AIAA/CEAS Aeroacoustics Conference*, 2019.